Applied Acoustics 71 (2010) 393–401

Contents lists available at ScienceDirect

Applied Acoustics

journal homepage: www.elsevier.com/locate/apacoust

A variational approach to free vibration analysis of shear deformable polygonal plates with variable thickness

María Virginia Quintana [a,*], Liz Graciela Nallim [a,b]

[a] ICMASA - INIQUI - Facultad de Ingeniería - Universidad Nacional de Salta, Av. Bolivia 5150, 4400 Salta, Argentina
[b] CONICET, Av. Rivadavia 1917, C1033AAJ, Buenos Aires, Argentina

ARTICLE INFO

Article history:
Received 13 August 2009
Received in revised form 27 November 2009
Accepted 1 December 2009
Available online 25 January 2010

Keywords:
Trapezoidal plates
Free vibration
Mindlin plates
Ritz method
Elastically restrained edges

ABSTRACT

This paper presents a simple and general variational approach for the study of the free vibration behaviour of polygonal isotropic plates with variable thickness. The Reissner–Mindlin plate theory is used to take into account the effects of shear deformation and rotary inertia in the analysis. Moreover, this theory allows obtaining greater accuracy of frequency coefficients corresponding to vibration higher modes, even for the thin plates.

The governing eigenvalue equation is obtained employing the Ritz method. The plate geometry is approximated by using non-orthogonal triangular co-ordinates, while sets of independent polynomials, expressed in these co-ordinates, are employed to approximate the displacement and rotation fields. The developed algorithm allows obtaining approximated analytical solutions for plates with different aspect ratios, thickness variation and boundary conditions, including edges elastically restrained by both translational and rotational springs. Therefore, a unified program has been easily implemented. Convergence and comparison analyzes are carried out to verify the reliability and accuracy of the numerical solutions. Finally, sets of parametric studies are performed and the results are given in graphical and tabular form.

Published by Elsevier Ltd.

1. Introduction

Polygonal tapered plates are commonly used in aerospace, civil and ocean engineering systems, electronic and optical equipment, mechanical elements, etc. In many cases, the design requirements include natural frequency constraints, so an accurate determination of the dynamical response is necessary as well as a realistic consideration of the involved geometric and mechanic parameters.

The references on this topic are very limited, especially when the boundary conditions are not the classical ones. Most of these publications deal with thin plates, as shown in Leissa's series of reviews [1–8]. However, the Classical Plate Theory which ignores the effect of transverse shear deformation becomes inadequate for the analysis of thick plates, resulting in an over-estimation of the free vibration frequencies. The First Order Theory based on Reissner [9] and Mindlin [10] assumes that the transverse shear strain distribution is constant through the plate thickness. For this reason a shear correction factor k, is needed to rectify the unrealistic variation of the shear strain/stress through the thickness and which ultimately define its corresponding shear strain energy.

As far as the literature about vibration of thick plates is concerned, Liew et al. [11] presented a very interesting review of the existing literature. Attention is mainly devoted to studies based on First Order Theory. In general, analytical studies on thick plates with shape different from rectangular are rather limited. This may be due to the difficulty in forming a simple and adequate deflection function which can be applied to the entire plate domain and satisfy the boundary conditions. To overcome this difficulty different techniques were developed and perfected. For instance, Karunasena et al. [12] used the Rayleigh–Ritz method based on two-dimensional polynomials and a set of basic functions that satisfy various boundary conditions to analyze the free vibration of thick cantilevered triangular plates based on the Mindlin shear deformation theory. Later on, Karunasena and Kitipornchai [13] extended the previous method to plate with any classical boundary conditions. Wu and Liu [14] applied the differential cubature method to solve the free vibration problems of arbitrary shaped thick plates. Zhong [15] used the triangular differential quadrature method to analyze the free flexural vibration of isosceles triangular Mindlin plates.

Often, the restraint along the boundaries of a real system cannot be actually represented by classical edge conditions such as simply supported, clamped and free. Therefore, it is of great importance to study the vibration characteristics of elastically restrained variable

* Corresponding author. Tel.: +54 3874255379.
E-mail addresses: virginiaquintana@argentina.com (M.V. Quintana), lnallim@unsa.edu.ar (L.G. Nallim).

0003-682X/$ - see front matter Published by Elsevier Ltd.
doi:10.1016/j.apacoust.2009.12.002

thickness plates. Compared to the large amount of researches on vibrating plates with classical boundary conditions the published works on thick plates with elastically restrained edge are limited to rectangular plate [16–19].

However, the more general problem of free vibration of polygonal tapered thick plates with edge elastically restrained against rotation and translation has received less attention, so the aim of this paper is to provide an approximated analytical solution to this problem based on first order shear deformation theory.

In a previous paper Nallim et al. [20], developed a general algorithm based on the Ritz method in conjunction with non-orthogonal triangular co-ordinates to express the geometry of quadrilateral plates in a simple form. That methodology was limited to the analysis of thin plates, since the Kirchhoff assumptions were used. The present work has been undertaken to extend and to generalize the mentioned algorithm to embrace thick plate including the effects of the shear deformation, the rotary inertia and no classical boundary conditions. The developed methodology is based on the Ritz method, where the transverse deflection and the rotations are approximated by sets of simple polynomials generated automatically.

Finally, it is clear that the use of triangular co-ordinates to approximate the geometry of the plate, makes the formulation obtained is limited to plates of trapezoidal shape (symmetrical or not symmetrical), allowing to obtain, as a special case, triangular plates. At the same time, analysis of plates with linearly varying thickness is included in this work. Other types of thickness variation could be considered without difficulty by means of the adequate incorporation of the functions that define these variations. Also, plates with discontinuous thickness can be treated simply by dividing the integration domain according of the discontinuities in the rigidities (see for instance Ref. [21]).

2. Analysis

The analyzed plate is shown in Fig. 1. Take into account the hypotheses of the first order shear deformation plate theory [9,10] the maximum kinetic energy of a freely vibrating plate expressed in a rectangular cartesian co-ordinate system is given by:

$$T_{\max} = \frac{1}{2}\rho\omega^2 \int_A h(x)[W^2 + \frac{h^2(x)}{12}(\phi_x^2 + \phi_y^2)]dA, \tag{1}$$

where ρ is the mass density of the plate material, $h(x)$ is the non-uniform plate thickness, ω is the radian frequency, $W(x,y)$ is the transverse deflection amplitude, $\phi_y(x,y)$ and $\phi_x(x,y)$ are the rotation about the x-axis and y-axis, respectively, and the integration is carried out over the entire plate domain A. In the present study the plate thickness varies in linear fashion as:

$$h(x) = h^{(1)} f(x), \tag{2}$$

$$f(x) = \left[1 + c_h\left(\frac{x}{l} - c_l\right)\right], \tag{3}$$

where $h^{(1)}$ is the value of h referred to edge 1, $h^{(2)} = h^{(1)}[1 + c_h(1 - c_l)]$ is the value of h referred to edge 2, $c_l = c/l$ and c_h is the taper parameter (see Fig. 1).

The maximum strain energy of the mechanical system is given by:

$$U_{\max} = U_{P,\max} + U_{R,\max} + U_{T,\max}, \tag{4}$$

where $U_{P,\max}$ is the maximum strain energy due to plate bending, which in rectangular co-ordinates is given by:

$$U_{P,\max} = \frac{1}{2}\int_A \left\{ D(x)\left\{ \left(\frac{\partial\phi_x}{\partial x} + \frac{\partial\phi_y}{\partial y}\right)^2 - 2(1-\mu)\left[\frac{\partial\phi_x}{\partial x}\frac{\partial\phi_y}{\partial y} - \frac{1}{4}\left(\frac{\partial\phi_x}{\partial y} + \frac{\partial\phi_y}{\partial x}\right)^2\right]\right\} + kGh(x)\left[\left(\phi_x + \frac{\partial W}{\partial x}\right)^2 + \left(\phi_y + \frac{\partial W}{\partial y}\right)^2\right]\right\} dA, \tag{5}$$

where k is the shear correction factor, $D(x)$ is the flexural rigidity and it is given by $D(x) = D^{(1)} f^3(x)$, $D^{(1)} = E(h^{(1)})^3 \big/ 12(1-\mu^2)$, in which E is the Young's modulus, μ is the Poisson's ratio and G is the shear modulus.

The maximum strain energies stored in the translational and rotational springs at the plate edges are, respectively, given by:

$$U_{T,\max} = \frac{1}{2}\oint_{\partial A} c_T(s) W^2 ds = \frac{1}{2}\sum_{i=1}^{4}\int_0^{l_i} c_{T_i} W^2 ds, \tag{6}$$

$$U_{R,\max} = \frac{1}{2}\oint_{\partial A} c_R(s)\phi_n^2 ds = \frac{1}{2}\sum_{i=1}^{4}\int_0^{l_i} c_{R_i}\phi_n^2 ds, \tag{7}$$

where ϕ_n denote the rotation about the corresponding co-ordinate and l_i is the length of side ∂A_i ($i = 1, \ldots, 4$).

2.1. The non-orthogonal right triangular co-ordinates

Let us introduce non-orthogonal right triangular co-ordinates u, v. They are related to the x, y co-ordinates by

$$u = \frac{x}{l}, \quad v = \frac{y}{x}\cot\alpha_1, \tag{8}$$

where $\tan\alpha_1$ is the slope of the upper side plate (see Fig. 1). After this co-ordinate transformation the two dimensional plate domain A is transformed into $\tilde{A} = \{(u,v), c_l \leqslant u \leqslant 1, \tan\alpha_2\cot\alpha_1 \leqslant v \leqslant 1\}$.

Applying the chain rule of differentiation, the first derivative of any function $f = f(x,y)$ in the two co-ordinate systems are related by

$$\begin{bmatrix} \frac{\partial f}{\partial x} \\ \frac{\partial f}{\partial y} \end{bmatrix} = \begin{bmatrix} \frac{1}{l} & -\frac{v}{ul} \\ 0 & \frac{1}{ul\tan\alpha_1} \end{bmatrix} \begin{bmatrix} \frac{\partial f}{\partial u} \\ \frac{\partial f}{\partial v} \end{bmatrix}. \tag{9}$$

Substituting $dx\,dy = ul^2\tan\alpha_1\,du\,dv$ into Eq. (1) the maximum kinetic energy becomes

$$T_{\max} = \frac{\rho h^{(1)} l^4 \tan\alpha_1}{2}\omega^2 \int_{c_l}^{1}\int_{v_0}^{1}\left[f(u)uW^2 + \frac{f^3(u)}{12}uh_l^2\left(\phi_x^2 + \phi_y^2\right)\right]du\,dv, \tag{10}$$

where $v_0 = \tan\alpha_2\cot\alpha_1$, $W = W(u,v) = \frac{W(x,y)}{l}$, $f(u) = [1 + c_h(u - c_l)]$ and $h_l = \frac{h^{(1)}}{l}$.

Substituting Eq. (9) and $dx\,dy = ul^2\tan\alpha_1\,du\,dv$ into Eq. (5) the maximum strain energy expression becomes

$$\begin{aligned} U_{P,\max} = \frac{D^{(1)}\tan\alpha_1}{2}\int_{c_l}^{1}\int_{v_0}^{1}\Bigg\{ & f^3(u)\left(u\left(\frac{\partial\phi_x}{\partial u}\right)^2 + \frac{2v^2\tan^2\alpha_1 + 1 - \mu}{2u\tan^2\alpha_1}\left(\frac{\partial\phi_x}{\partial v}\right)^2 \right. \\ & + \frac{(1-\mu)u}{2}\left(\frac{\partial\phi_y}{\partial u}\right)^2 + \frac{2 + (1-\mu)v^2\tan^2\alpha_1}{2u\tan^2\alpha_1}\left(\frac{\partial\phi_y}{\partial v}\right)^2 - 2v\frac{\partial\phi_x}{\partial u}\frac{\partial\phi_x}{\partial v} \\ & + \frac{2\mu}{\tan\alpha}\frac{\partial\phi_x}{\partial u}\frac{\partial\phi_y}{\partial v} - \frac{v(1+\mu)}{u\tan\alpha}\frac{\partial\phi_x}{\partial v}\frac{\partial\phi_y}{\partial v} + \frac{1-\mu}{\tan\alpha}\frac{\partial\phi_y}{\partial u}\frac{\partial\phi_x}{\partial v} \\ & \left. - v(1-\mu)\frac{\partial\phi_y}{\partial u}\frac{\partial\phi_y}{\partial v}\right) + \gamma f(u)\left(u(\phi_x)^2 + u(\phi_y)^2 + u\left(\frac{\partial W}{\partial u}\right)^2\right. \\ & + \frac{v^2\tan^2\alpha_1 + 1}{u\tan^2\alpha_1}\left(\frac{\partial W}{\partial v}\right)^2 + 2u\frac{\partial W}{\partial u}\phi_x - 2v\frac{\partial W}{\partial v}\phi_x - 2v\frac{\partial W}{\partial u}\frac{\partial W}{\partial v} \\ & \left.\left. + \frac{2}{\tan\alpha}\frac{\partial W}{\partial v}\phi_y\right)\right\} du\,dv, \end{aligned} \tag{11}$$

where $\gamma = \frac{kGh^{(1)}l^2}{D^{(1)}} = \frac{6k(1-\mu)}{h_l^2}$.

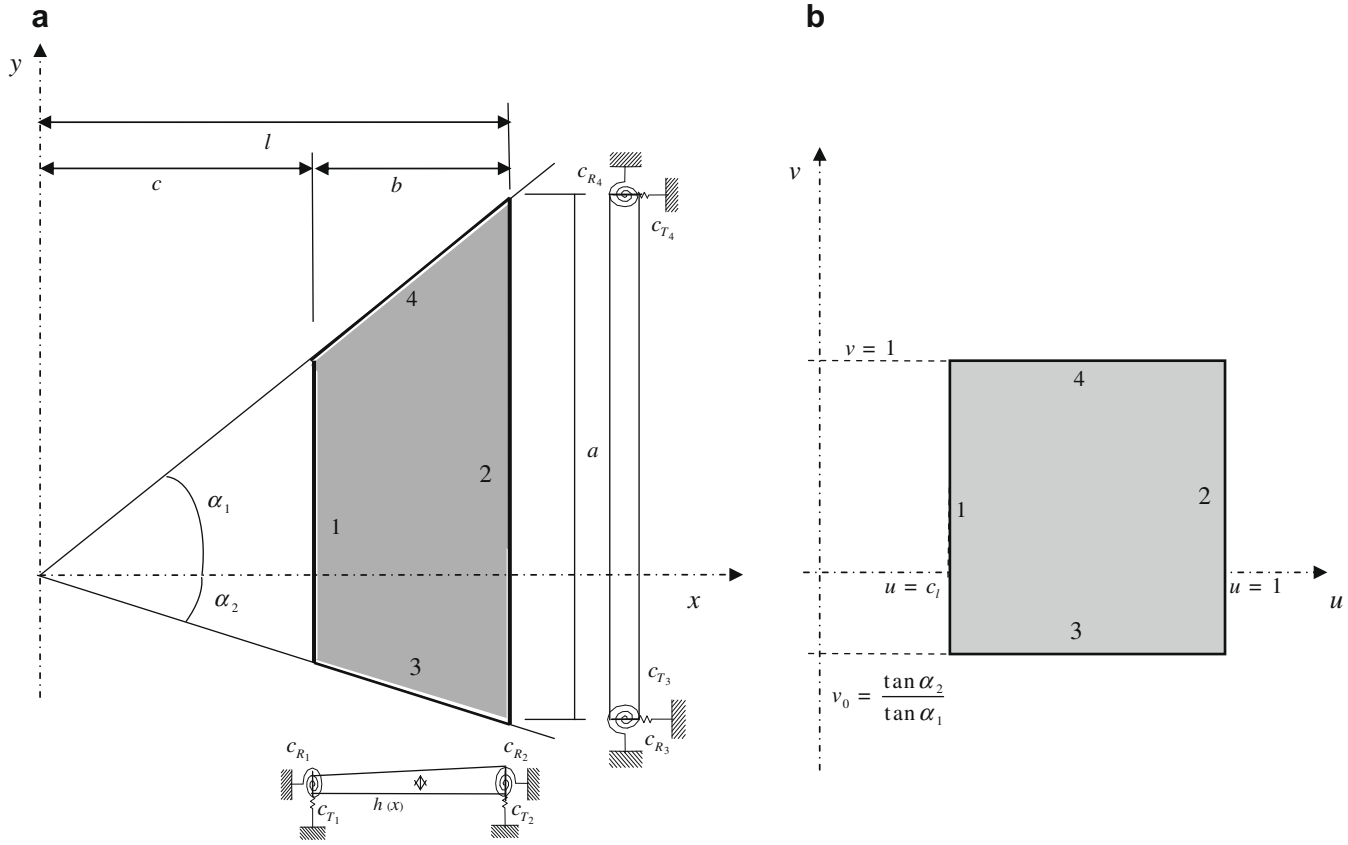

Fig. 1. Geometry of the trapezoidal plate.

Substituting the change of variables (9) into Eq. (6) the maximum strain energy stored in the translational springs at the plate edges becomes

$$U_{T,\max} = \frac{D^{(1)}\tan\alpha_1}{2}\left(c_l T_1 \int_{v_0}^{1} W^2\big|_{u=c_l} dv + T_2 \int_{v_0}^{1} W^2\big|_{u=1} dv + \frac{T_3}{\tan\alpha_1 \cos\alpha_2}\int_{c_l}^{1} W^2\big|_{v=v_0} du + \frac{T_4}{\sin\alpha_1}\int_{c_l}^{1} W^2\big|_{v=1} du\right), \tag{12}$$

where $T_i = \frac{c_{T_i} l^3}{D^{(1)}}$.

Finally, using the mentioned change of variables in Eq. (7) the maximum strain energy stored in the rotational springs at the plate edges becomes

$$U_{R,\max} = \frac{D^{(1)}\tan\alpha_1}{2}\left(c_l R_1 \int_{v_0}^{1} \phi_x^2\big|_{u=c_l} dv + R_2 \int_{v_0}^{1} \phi_x^2\big|_{u=1} dv + \frac{R_3}{\tan\alpha_1 \cos\alpha_2}\int_{c_l}^{1} \phi_y^2\big|_{v=v_0} du + \frac{R_4}{\sin\alpha_1}\int_{c_l}^{1} \phi_y^2\big|_{v=1} du\right), \tag{13}$$

where $R_i = \frac{c_{R_i} l}{D^{(1)}}$.

2.2. Trial functions

The plate transverse deflections $W(u, v)$ and the rotations $\phi_y(u, v)$ and $\phi_x(u, v)$ can be represented by means of simple polynomials as

$$W(u,v) = \sum_{i=1}^{M}\sum_{j=1}^{N} c_{ij}^{(W)} p(u)_i^{(W)} q(v)_j^{(W)}, \tag{14}$$

$$\phi_x(u,v) = \sum_{i=1}^{M}\sum_{j=1}^{N} c_{ij}^{(\phi_x)} p(u)_i^{(\phi_x)} q(v)_j^{(\phi_x)}, \tag{15}$$

$$\phi_y(u,v) = \sum_{i=1}^{M}\sum_{j=1}^{N} c_{ij}^{(\phi_y)} p(u)_i^{(\phi_y)} q(v)_j^{(\phi_y)}, \tag{16}$$

where the $c_{ij}^{(W)}$, $c_{ij}^{(\phi_x)}$ and $c_{ij}^{(\phi_y)}$ are the unknown coefficients to be determined by the application of the Ritz method. It is sufficient that the trial functions satisfy the geometric boundary conditions since the natural boundary conditions will be exactly satisfied as the number of functions approaches infinity [22]. In consequence, the first members of the sets of polynomials $\{p(u)_i^{(W)}\}$, $\{q(v)_j^{(W)}\}$, $\{p(u)_i^{(\phi_x)}\}$, $\{q(v)_j^{(\phi_x)}\}$, $\{p(u)_i^{(\phi_y)}\}$ and $\{q(v)_j^{(\phi_y)}\}$ are obtained as the simplest polynomials that satisfy all the geometric boundary conditions.

The polynomials of higher order are generated using the following simple procedure, i.e.

$$p(u)_i^{(W)} = p(u)_1^{(W)} u^{i-1}, \quad i = 2,\ldots,M,$$
$$p(u)_i^{(\phi_x)} = p(u)_1^{(\phi_x)} u^{i-1}, \quad i = 2,\ldots,M,$$
$$p(u)_i^{(\phi_y)} = p(u)_1^{(\phi_y)} u^{i-1}, \quad i = 2,\ldots,M,$$

The polynomial sets along the v direction are generated by using the same procedure.

Let us introduce the terminology to be used throughout the remainder of the paper for describing the boundary conditions of the polygonal plates considered. The symbolism **CSFE**, for example, identifies a polygonal plate with edges: (1) clamped (2) simply supported (3) free and (4) elastically restrained (see Fig. 1). In the particular case when the plate has a triangular shape, the edge 1 disappears.

In the present paper, plates having a variety of boundary conditions are considered and the starting trial functions used are given in Appendix A.

3. The Ritz method

The Ritz method require the minimization of the following energy functional

$$\Pi = U_{\max} - T_{\max}, \tag{17}$$

where $T_{\max}$ and $U_{\max}$ are given by the expressions (10)–(13), respectively.

Substituting Eqs. (14)–(16) into Eq. (17) and minimizing with respect to the unknown coefficients $c_{ij}^{(W)}$, $c_{ij}^{(\phi_x)}$ and $c_{ij}^{(\phi_y)}$ by means of the necessary conditions

$$\frac{\partial \Pi}{\partial c_{ij}^{(W)}} = 0, \quad \frac{\partial \Pi}{\partial c_{ij}^{(\phi_x)}} = 0, \quad \frac{\partial \Pi}{\partial c_{ij}^{(\phi_y)}} = 0, \tag{18}$$

the following governing eigenvalue equation is obtained:

$$([K] - \Omega^2[M])\{\bar{c}\} = \{0\}, \tag{19}$$

where $\Omega = \omega l^2\sqrt{\rho h^{(1)}/D^{(1)}}$ is the non-dimensional frequency parameter, $[K]$ is the stiffness matrix of the plate, $[M]$ is the mass matrix of the plate and $\{\bar{c}\}$ is the column matrix of the unknown constants. The stiffness and the mass matrices are, respectively, given by

$$[K] = \begin{bmatrix} [K^{WW}] & [K^{W\phi_x}] & [K^{W\phi_y}] \\ & [K^{\phi_x\phi_x}] & [K^{\phi_x\phi_y}] \\ \text{sym.} & & [K^{\phi_y\phi_y}] \end{bmatrix} \quad \text{and}$$

$$[M] = \begin{bmatrix} [M^{WW}] & [0] & [0] \\ & [M^{\phi_x\phi_x}] & [0] \\ \text{sym.} & & [M^{\phi_y\phi_y}] \end{bmatrix}, \tag{20}$$

where:

$$\begin{aligned} K_{ijmn}^{WW} = \int_{c_l}^1 \int_{v_0}^1 \gamma f(u) \Bigg(& u \frac{\partial p_i^{(W)}}{\partial u} q_j^{(W)} \frac{\partial p_m^{(W)}}{\partial u} q_n^{(W)} \\ & + \frac{v^2 \tan^2\alpha_1 + 1}{u \tan^2\alpha_1} p_i^{(W)} \frac{\partial q_j^{(W)}}{\partial v} p_m^{(W)} \frac{\partial q_n^{(W)}}{\partial v} \\ & - v\left(\frac{\partial p_i^{(W)}}{\partial u} q_j^{(W)} p_m^{(W)} \frac{\partial q_n^{(W)}}{\partial v} + p_i^{(W)} \frac{\partial q_j^{(W)}}{\partial v} \frac{\partial p_m^{(W)}}{\partial u} q_n^{(W)} \right) \Bigg) du\, dv \\ & + c_l T_1 \int_{v_0}^1 (p_i^{(W)} q_j^{(W)} p_m^{(W)} q_n^{(W)})\Big|_{u=c_l} dv \\ & + T_2 \int_{v_0}^1 (p_i^{(W)} q_j^{(W)} p_m^{(W)} q_n^{(W)})\Big|_{u=1} dv \\ & + \frac{T_3}{\tan\alpha_1 \cos\alpha_2} \int_{c_l}^1 (p_i^{(W)} q_j^{(W)} p_m^{(W)} q_n^{(W)})\Big|_{v=v_0} du \\ & + \frac{T_4}{\sin\alpha_1} \int_{c_l}^1 (p_i^{(W)} q_j^{(W)} p_m^{(W)} q_n^{(W)})\Big|_{v=1} du, \end{aligned} \tag{21}$$

$$K_{ijmn}^{W\phi_x} = \int_{c_l}^1 \int_{v_0}^1 \gamma f(u) \left\{ u \frac{\partial p_i^{(W)}}{\partial u} q_j^{(W)} p_m^{(\phi_x)} q_n^{(\phi_x)} - v p_i^{(W)} \frac{\partial q_j^{(W)}}{\partial v} p_m^{(\phi_x)} q_n^{(\phi_x)} \right) \Bigg\} du\, dv, \tag{22}$$

$$K_{ijmn}^{W\phi_y} = \int_{c_l}^1 \int_{v_0}^1 \gamma f(u) \frac{1}{\tan\alpha_1} p_i^{(W)} \frac{\partial q_j^{(W)}}{\partial v} p_m^{(\phi_y)} q_n^{(\phi_y)} du\, dv, \tag{23}$$

$$\begin{aligned} K_{ijmn}^{\phi_x\phi_x} = \int_{c_l}^1 \int_{v_0}^1 \Bigg\{ & f^3(u) \Bigg(\frac{2v^2 \tan^2\alpha_1 + 1 - \mu}{2u \tan^2\alpha_1} p_i^{(\phi_x)} \frac{\partial q_j^{(\phi_x)}}{\partial v} p_m^{(\phi_x)} \frac{\partial q_n^{(\phi_x)}}{\partial v} \\ & + u \frac{\partial p_i^{(\phi_x)}}{\partial u} q_j^{(\phi_x)} \frac{\partial p_m^{(\phi_x)}}{\partial u} q_n^{(\phi_x)} - v\Bigg(\frac{\partial p_i^{(\phi_x)}}{\partial u} q_j^{(\phi_x)} p_m^{(\phi_x)} \frac{\partial q_n^{(\phi_x)}}{\partial v} \\ & + p_i^{(\phi_x)} \frac{\partial q_j^{(\phi_x)}}{\partial v} \frac{\partial p_m^{(\phi_x)}}{\partial u} q_n^{(\phi_x)} \Bigg) \Bigg) + \gamma f(u) u p_i^{(\phi_x)} q_j^{(\phi_x)} p_m^{(\phi_x)} q_n^{(\phi_x)} \Bigg\} du\, dv \\ & + c_l R_1 \int_{v_0}^1 \left(p_i^{(\phi_x)} q_j^{(\phi_x)} p_m^{(\phi_x)} q_n^{(\phi_x)} \right)\Big|_{u=c_l} dv \\ & + R_2 \int_{v_0}^1 \left(p_i^{(\phi_x)} q_j^{(\phi_x)} p_m^{(\phi_x)} q_n^{(\phi_x)} \right)\Big|_{u=1} dv, \end{aligned} \tag{24}$$

$$\begin{aligned} K_{ijmn}^{\phi_x\phi_y} = \int_{c_l}^1 \int_{v_0}^1 \Bigg\{ & f^3(u) \Bigg(\frac{\mu}{\tan\alpha_1} \frac{\partial p_i^{(\phi_x)}}{\partial u} q_j^{(\phi_x)} p_m^{(\phi_y)} \frac{\partial q_n^{(\phi_y)}}{\partial v} \\ & - \frac{v(1+\mu)}{2u\tan\alpha_1} p_i^{(\phi_x)} \frac{\partial q_j^{(\phi_x)}}{\partial v} p_m^{(\phi_y)} \frac{\partial q_n^{(\phi_y)}}{\partial v} + \frac{v(1-\mu)}{2\tan\alpha_1} p_i^{(\phi_x)} \frac{\partial q_j^{(\phi_x)}}{\partial v} \frac{\partial p_m^{(\phi_y)}}{\partial u} q_n^{(\phi_y)} \Bigg) \Bigg\} du\, dv, \end{aligned} \tag{25}$$

$$\begin{aligned} K_{ijmn}^{\phi_y\phi_y} = \int_{c_l}^1 \int_{v_0}^1 \Bigg\{ & f^3(u) \Bigg(\frac{2 + (1-\mu)v^2 \tan^2\alpha_1}{2u \tan^2\alpha_1} p_i^{(\phi_y)} \frac{\partial q_j^{(\phi_y)}}{\partial v} p_m^{(\phi_y)} \frac{\partial q_n^{(\phi_y)}}{\partial v} \\ & + u \frac{(1-\mu)}{2} \frac{\partial p_i^{(\phi_y)}}{\partial u} q_j^{(\phi_y)} \frac{\partial p_m^{(\phi_y)}}{\partial u} q_n^{(\phi_y)} \\ & - v \frac{(1-\mu)}{2} \Big(\frac{\partial p_i^{(\phi_y)}}{\partial u} q_j^{(\phi_y)} p_m^{(\phi_y)} \frac{\partial q_n^{(\phi_y)}}{\partial v} p_i^{(\phi_y)} \frac{\partial q_j^{(\phi_y)}}{\partial v} \frac{\partial p_m^{(\phi_y)}}{\partial u} q_n^{(\phi_y)} \Bigg) \Bigg) \\ & + \gamma f(u) u p_i^{(\phi_y)} q_j^{(\phi_y)} p_m^{(\phi_y)} q_n^{(\phi_y)} \Bigg\} du\, dv \\ & + \frac{R_3}{\tan\alpha_1 \cos\alpha_2} \int_{c_l}^1 \left(p_i^{(\phi_y)} q_j^{(\phi_y)} p_m^{(\phi_y)} q_n^{(\phi_y)} \right)\Big|_{v=v_0} du \\ & + \frac{R_4}{\sin\alpha_1} \int_{c_l}^1 \left(p_i^{(\phi_y)} q_j^{(\phi_y)} p_m^{(\phi_y)} q_n^{(\phi_y)} \right)\Big|_{v=1} du, \end{aligned} \tag{26}$$

$$M_{ijmn}^{WW} = \int_{c_l}^1 \int_{v_0}^1 f(u) u p_i^{(W)} q_j^{(W)} p_m^{(W)} q_n^{(W)} du\, dv, \tag{27}$$

$$M_{ijmn}^{\phi_x\phi_x} = \int_{c_l}^1 \int_{v_0}^1 \frac{f^3(u)}{12} u h_l^2 p_i^{(\phi_x)} q_j^{(\phi_x)} p_m^{(\phi_x)} q_n^{(\phi_x)} du\, dv, \tag{28}$$

$$M_{ijmn}^{\phi_y\phi_y} = \int_{c_l}^1 \int_{v_0}^1 \frac{f^3(u)}{12} u h_l^2 p_i^{(\phi_y)} q_j^{(\phi_y)} p_m^{(\phi_y)} q_n^{(\phi_y)} du\, dv. \tag{29}$$

4. Numerical results

In order to establish the accuracy and applicability of the described approach, numerical results were computed for a number

Table 1
Convergence study of the first four values of the frequency parameters $\Omega/\pi^2 = \omega/\pi^2 l^2\sqrt{\rho h^{(1)}/D^{(1)}}$ for FCF triangular plates ($\tan\alpha_1 = 0.5$, $\tan\alpha_2 = 0$, $c_l = 0$) with uniform thickness ($c_h = 0$) and for two different thickness ratios $h_l = 0.05,\ 0.1$.

h_l	$M \times N$	Ω_1/π^2	Ω_2/π^2	Ω_3/π^2	Ω_4/π^2
0.05	5 × 5	2.200	6.657	10.867	15.673
	6 × 6	2.192	5.888	10.730	14.319
	7 × 7	2.184	5.867	10.676	11.609
	8 × 8	2.181	5.791	10.663	11.503
	9 × 9	2.180	5.782	10.636	11.193
	10 × 10	2.180	5.778	10.629	11.178
	FEM	2.176	5.757	10.544	11.185
0.1	5 × 5	2.098	5.702	9.104	12.552
	6 × 6	2.093	5.245	9.005	11.135
	7 × 7	2.088	5.223	8.979	9.806
	8 × 8	2.087	5.188	8.971	9.703
	9 × 9	2.086	5.183	8.965	9.575
	10 × 10	2.086	5.182	8.962	9.565
	FEM	2.119	5.456	9.461	10.099

Table 2
Comparison study of the values of the frequency parameter $\Omega/\pi^2 = \omega/\pi^2 l^2\sqrt{\rho h^{(1)}/D^{(1)}}$ for triangular plates ($c_l = 0, \tan\alpha_2 = 0,\ c_h = 0$) with different boundary conditions.

Boundary conditions	$\tan\alpha_1$	h_l		Ω_1/π^2	Ω_2/π^2	Ω_3/π^2	Ω_4/π^2
CCC	1	0.001	Present	9.504	16.033	19.788	24.955
			Karunasena and Kitipornchai [13]	9.503	15.988	19.741	24.655
	2	0.001	Present	5.416	8.386	11.639	12.478
			Karunasena and Kitipornchai [13]	5.415	8.355	11.518	12.357
SSS	1	0.001	Present	5.000	10.012	13.025	17.036
			Karunasena and Kitipornchai [13]	5.000	9.999	13.000	17.005
	2	0.001	Present	2.813	5.064	7.760	8.374
			Karunasena and Kitipornchai [13]	2.813	5.054	7.569	8.241
FSC	0.5	0.001	Present	9.217	18.284	26.703	30.564
			Karunasena and Kitipornchai [13]	9.214	18.156	26.490	29.184
		0.2	Present	5.286	8.402	11.243	11.810
			Karunasena and Kitipornchai [13]	5.285	8.400	11.236	11.746
	1	0.001	Present	3.220	7.379	9.575	13.600
			Karunasena and Kitipornchai [13]	3.220	7.376	9.559	13.486
		0.2	Present	2.428	4.813	5.562	7.527
			Karunasena and Kitipornchai [13]	2.428	4.812	5.561	7.523
FCF	0.5	0.05	Present	2.180	5.783	10.636	11.193
			Karunasena and Kitipornchai [13]	2.179	5.773	10.621	11.164
		0.2	Present	1.840	3.972	6.073	6.890
			Karunasena and Kitipornchai [13]	1.840	3.972	6.072	6.882
	2	0.05	Present	0.167	0.715	1.218	1.740
			Karunasena and Kitipornchai [13]	0.167	0.715	1.216	1.739
		0.2	Present	0.164	0.670	1.000	1.530
			Karunasena and Kitipornchai [13]	0.164	0.670	1.000	1.530

of plate problems for which comparison values were available in the literature. Additionally, new numerical results were generated for several problems which also can serve as supplement database for variable thickness thick plates. The frequency coefficients Ω were computed varying the parameters involved, such as the taper parameter, aspect ratio that defines the shape of the trapezoidal plate as well as different boundary conditions. All calculations have been performed taking the Poisson's ratio $\mu = 0.3$ and the shear correction factor $k = 5/6$.

The computations in this paper were performed by using Maple (TM). The routine computes in exact way the definite integral over the straight line from a to b. The eigenvalues are computed by the QR method. The matrix is first balanced and transformed into upper Hessenberg form. Then the eigenvalues are computed. If the matrix is symmetric then the routine will handle the matrix specially (using a faster algorithm) [23].

4.1. Validation and convergence studies

Simple polynomials were proposed in the previous section as trial functions for analyzing the free vibration of thick plates using the Ritz method. In order to establish the accuracy of the present method and the trial functions proposed, comparison and convergence studies are carried out in this section.

Table 3
Comparison study of the values of the frequency parameter $\lambda = \omega/(2\pi)a^2\sqrt{\rho h^{(1)}/D^{(1)}}$ for uniform trapezoidal plates ($h_l = 0.001,\ c_h = 0$) with different boundary conditions.

$\tan\alpha_1$	$\tan\alpha_2$	c_l		λ_1	λ_2	λ_3	λ_4
Boundary conditions: FCFF							
			Nallim et. al. [20]	1.07	4.64	4.65	11.12
			Nallim et. al. [20]	0.82	3.53	3.88	9.18
			Nallim et. al. [20]	0.70	2.65	3.67	7.30
Boundary conditions: CFCC							
			Nallim et. al. [20]	6.54	13.80	17.36	24.21
		0.2	Present	6.54	13.80	17.37	24.25
			Nallim et. al. [20]	6.54	13.80	17.35	24.18
			Nallim et. al. [20]	9.26	20.23	28.71	37.32
		0.2	Present	9.29	20.23	29.28	37.39
			Nallim et. al. [20]	9.29	20.23	29.41	37.71

Table 4
The first four values of the frequency parameter $\lambda = \omega/(2\pi)a^2\sqrt{\rho h^{(1)}/D^{(1)}}$ for trapezoidal plates ($c_h = 0$) with two different boundary conditions.

$\tan\alpha_1$	$\tan\alpha_2$	h_l	c_l	λ_1	λ_2	λ_3	λ_4
Boundary conditions: FFFF							
			0.2	31.632	34.167	34.758	76.131
			0.4	33.890	45.587	56.747	85.205
		0.05	0	26.129	30.431	33.440	63.944
			0.2	30.652	33.442	33.837	72.403
			0.4	32.795	33.095	55.172	80.176
		0.2	0	22.346	24.652	27.559	47.540
			0.2	25.016	27.237	28.375	50.327
			0.4	26.631	27.390	42.702	55.199
			0.2	36.871	76.240	112.509	148.754
			0.4	35.324	76.153	118.542	152.423
		0.05	0	36.691	75.710	109.885	142.282
			0.2	36.695	75.540	110.617	145.865
			0.4	35.169	74.657	115.049	148.530
		0.2	0	35.384	70.175	97.425	123.771
			0.2	35.379	70.336	97.656	126.420
			0.4	33.987	69.891	98.664	131.238
Boundary conditions: SFCF							
			0.2	8.318	32.168	36.270	83.749
			0.4	9.008	35.811	46.197	87.945
		0.05	0	8.200	29.779	35.129	72.384
			0.2	8.200	30.903	35.176	79.033
			0.4	8.806	34.595	44.236	83.029
		0.2	0	7.593	23.176	27.346	49.570
			0.2	7.529	23.876	27.399	53.223
			0.4	7.882	26.551	33.392	54.770
			0.2	13.338	45.951	95.118	145.578
			0.4	19.288	49.340	113.784	185.325
		0.05	0	10.870	44.746	76.554	112.567
			0.2	12.927	45.423	92.050	137.552
			0.4	18.439	48.354	109.962	177.350
		0.2	0	10.673	42.504	66.209	99.875
			0.2	12.340	42.720	80.948	111.897
			0.4	17.397	44.651	99.359	141.996

The convergence studies have been undertaken for uniform thickness FCF ($\tan\alpha_1 = 0.5, \tan\alpha_2 = 0$) triangular plates for two different thickness ratios $h_l = 0.05,\ 0.1$. Results of the first four values of the frequency parameter $\Omega/\pi^2 = \omega/\pi^2 l^2\sqrt{\rho h^{(1)}/D^{(1)}}$ are given in Table 1. It can be seen that eigenvalue converge monotonically from above as the increase of the number of the terms in the trial functions. The rate of convergence is faster for plates with a higher thickness ratio. Besides, results obtained using a

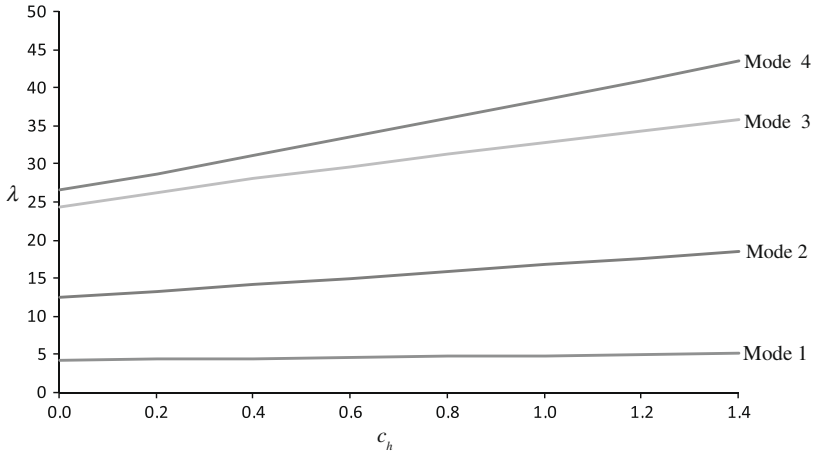

Fig. 2. Variation of frequency parameters $\lambda = \omega/(2\pi)a^2\sqrt{\rho h^{(1)}/D^{(1)}}$ with respect to the taper parameter c_h for the first four modes of free vibration of polygonal thick plate ($\tan\alpha_1 = 2,\ \tan\alpha_2 = -0.5,\ c_l = 0.2,\ h_l = 0.001$). The boundary conditions are SFFC.

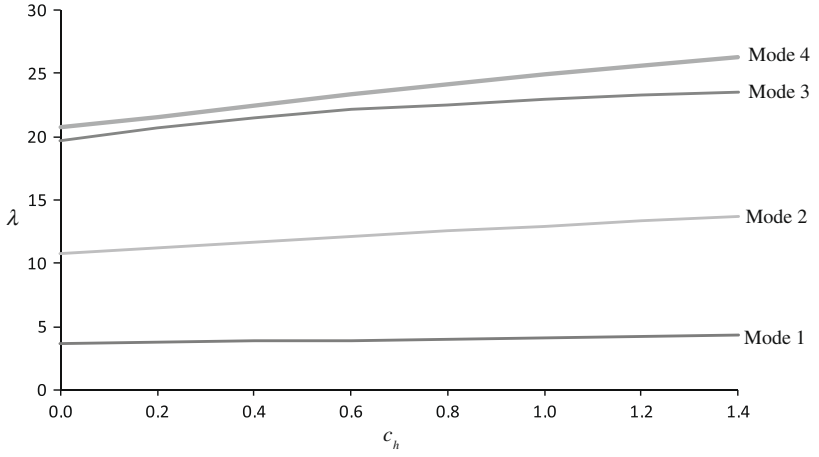

Fig. 3. Variation of frequency parameters $\lambda = \omega/(2\pi)a^2\sqrt{\rho h^{(1)}/D^{(1)}}$ with respect to the taper parameter c_h for the first four modes of free vibration of polygonal thick plate ($\tan\alpha_1 = 2,\ \tan\alpha_2 = -0.5,\ c_l = 0.2,\ h_l = 0.2$). The boundary conditions are SFFC.

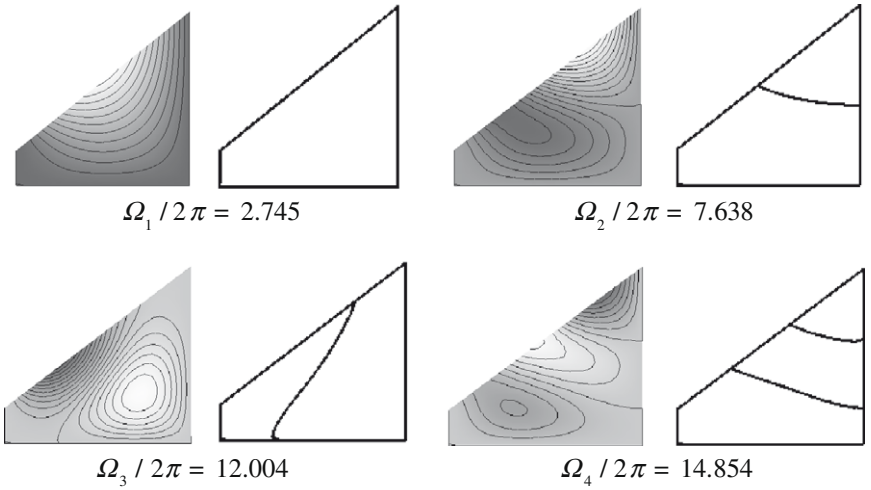

Fig. 4. Mode shapes and nodal patterns of a CSSF polygonal uniform plate with $\tan\alpha_1 = 1,\ \tan\alpha_2 = 0,\ c_l = 0.2,\ h_l = 0.001$ and $c_h = 0$.

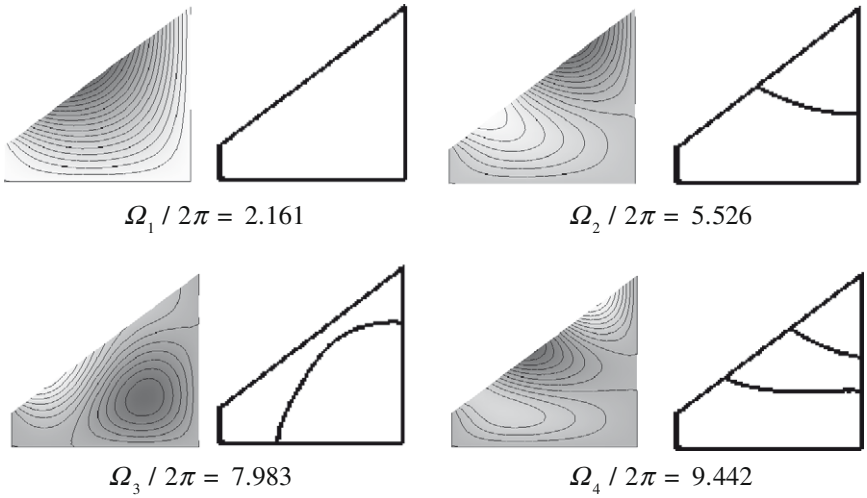

Fig. 5. Mode shapes and nodal patterns of a CSSF trapezoidal uniform plate with $\tan\alpha_1 = 1$, $\tan\alpha_2 = 0$, $c_l = 0.2$, $h_l = 0.2$ and $c_h = 0$.

FEM package SAP 2000 advanced 9.0.3 [24] have been included en Table 1. In this case, 100 thick plate elements have been used. The agreement with FEM is good from an engineering viewpoint.

The accuracy of the results obtained with the present method is next demonstrated by comparing them with some selected values published by other researchers. Table 2 depicts the first four values of frequency parameter Ω/π^2 for triangular plates subjected to four types of combinations of edge conditions, uniform thickness ($c_h = 0$) and different thickness ratios. The comparison with the results of Karunasena and Kitipornchai [13] shows a very close agreement.

The second set of results, available for comparison, corresponds to the case of trapezoidal plate ($h_l = 0.001, c_h = 0$) with different combinations of classical edge conditions. The non-dimensional frequency coefficients

$$\lambda = \frac{\omega l^2}{2\pi}(\tan\alpha_1 - \tan\alpha_2)^2\sqrt{\rho h^{(1)}/D^{(1)}} = \frac{\omega a^2}{2\pi}\sqrt{\rho h^{(1)}/D^{(1)}},$$

computed with the present approach are tabulated in Table 3. The comparison with those of Ref. [20] shows an excellent agreement. This comparison also authenticates the validity of the present method for thin trapezoidal plates.

4.2. Numerical results and discussion

In this section, numerical results of frequency parameters are obtained for a range of trapezoidal and triangular plates and for different combination of edge support conditions. A great number of problems were solved and since the number of cases is extremely large, results are presented for only a few representative cases.

Table 5
The first five values of the frequency parameter $\Omega = \omega l^2\sqrt{\rho h^{(1)}/D^{(1)}}$ of an isosceles triangular plate ($\theta_1 = -\theta_2 = 15°$, $c_h = 0$) and edges 1–3 elastically restrained against rotation ($R = R_1 = R_2 = R_3$) and translation ($T = T_1 = T_2 = T_3$) for thickness ratio $h_l = 0.1$.

T	R	Ω_1	Ω_2	Ω_3	Ω_4	Ω_5
∞	0	81.142	138.823	192.326	201.481	269.797
	1	84.315	141.451	194.531	203.690	271.575
	10	100.085	155.445	206.559	216.032	281.386
	50	115.392	170.387	219.853	230.269	292.478
	100	119.280	174.379	223.467	234.254	295.539
	∞	124.184	179.523	228.152	239.499	299.539
100	0	26.694	37.164	41.731	55.201	68.119
	1	26.896	37.639	45.770	56.289	76.793
	10	27.510	38.707	55.660	59.233	88.253
	50	27.821	39.124	60.577	61.016	90.991
	100	27.878	39.196	60.819	62.074	91.526
	∞	27.942	39.275	61.087	63.286	92.136
50	0	19.726	27.636	29.824	44.482	59.569
	1	19.812	28.384	35.507	45.669	69.788
	10	20.030	29.930	48.215	48.899	79.829
	50	20.127	30.481	50.368	54.827	83.005
	100	20.144	30.573	50.630	56.118	83.626
	∞	20.163	30.672	50.921	57.592	84.336
10	0	9.323	13.456	13.511	30.683	51.559
	1	9.331	14.664	23.768	32.367	63.538
	10	9.342	16.579	36.810	41.017	72.673
	50	9.346	17.147	38.768	49.141	76.341
	100	9.346	17.236	39.117	50.693	77.057
	∞	9.347	17.332	39.504	52.452	77.877

Table 6
The first five values of the frequency parameter $\Omega = \omega l^2\sqrt{\rho h^{(1)}/D^{(1)}}$ of an isosceles triangular plate ($\theta_1 = -\theta_2 = 15°$, $c_h = 0$) and edges 1–3 elastically restrained against rotation ($R = R_1 = R_2 = R_3$) and translation ($T = T_1 = T_2 = T_3$) for thickness ratio $h_l = 0.05$.

T	R	Ω_1	Ω_2	Ω_3	Ω_4	Ω_5
∞	0	91.701	166.692	241.028	256.057	359.283
	1	95.726	170.576	244.575	259.829	362.620
	10	117.711	193.693	266.644	283.722	384.300
	50	143.427	224.669	298.472	319.690	418.483
	100	150.937	234.528	309.055	332.144	430.659
	∞	161.152	248.560	324.425	350.792	449.110
100	0	26.907	37.741	42.975	56.982	74.473
	1	27.112	38.212	47.103	58.111	83.455
	10	27.744	39.316	57.846	61.320	94.792
	50	28.068	39.768	62.869	64.181	97.032
	100	28.128	39.847	63.154	65.492	99.014
	∞	28.195	39.935	63.473	67.023	99.841
50	0	19.815	27.984	30.649	45.757	65.760
	1	19.902	28.731	36.545	47.004	76.365
	10	20.124	30.322	50.341	50.544	86.262
	50	20.224	30.904	52.230	58.075	90.277
	100	20.241	31.002	52.538	59.651	91.091
	∞	20.260	31.109	52.883	61.482	92.035
10	0	9.335	13.617	13.804	31.662	57.712
	1	9.343	14.774	24.624	33.447	70.110
	10	9.354	16.730	38.303	43.210	79.156
	50	9.358	17.318	40.524	52.575	83.708
	100	9.359	17.411	40.927	54.437	84.626
	∞	9.360	17.511	41.377	56.585	85.693

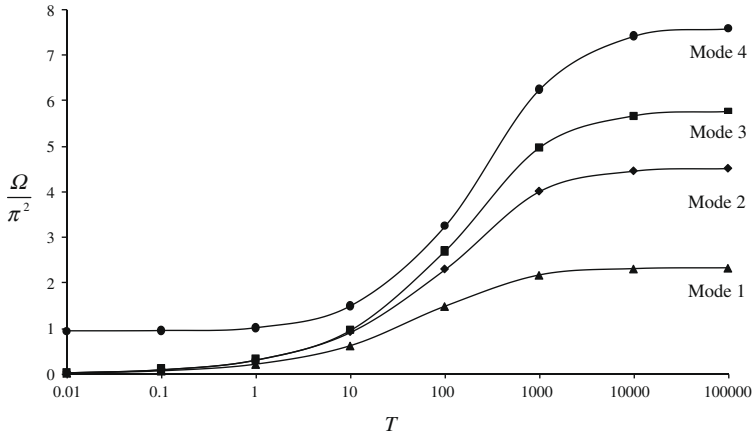

Fig. 6. Variation of the first four frequency parameter $\Omega/\pi^2 = \omega/\pi^2 l^2\sqrt{\rho h^{(1)}/D^{(1)}}$ with respect to translational restraint parameters $T = T_2 = T_3 = T_4$ for a triangular uniform plate $(\tan\alpha_1 = 1,\ \tan\alpha_2 = -1,\ c_l = 0,\ h_l = 0.1)$, $R_2 = R_3 = R_4 = 0$.

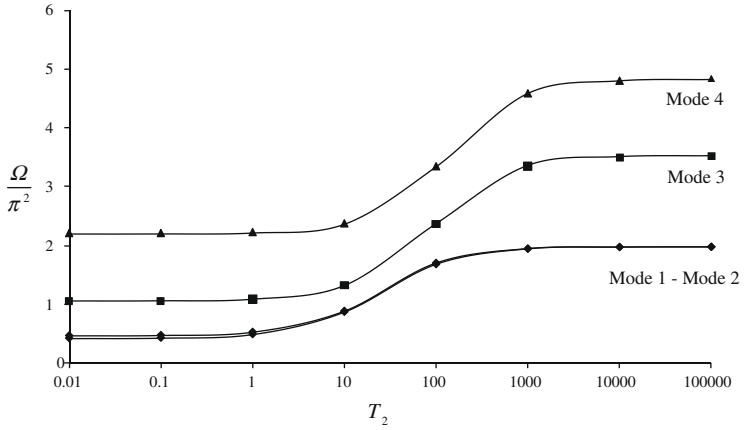

Fig. 7. Variation of the first four frequency parameter $\Omega/\pi^2 = \omega/\pi^2 l^2\sqrt{\rho h^{(1)}/D^{(1)}}$ with respect to translational restraint parameters T_2 $(R_2 = 0)$ for a CEFF trapezoidal plate $(\tan\alpha_1 = 1,\ \tan\alpha_2 = -1,\ c_l = 0.3,\ h_l = 0.1)$.

Table 4 presents the first four values of the frequency parameter λ for trapezoidal plates with different values of the angles α_1 and α_2. Two different boundary conditions were considered: FFFF and SFCF and three values of the geometrical parameters $h_l = 0.001$, 0.05, 0.2. Figs. 2 and 3 show the variation of the frequency parameters λ with the taper parameter c_h for the first four modes of free vibration of polygonal plates $(\tan\alpha_1 = 2, \tan\alpha_2 = -0.5)$. The boundary conditions are SFFC and the geometrical parameter is $c_l = 0.2$. From these figures, it appears that the variation of the frequency with the taper parameter is linear for the modes one to four. It is interesting to point out that the curve slope increases as the mode of vibration increases in both cases.

The first four mode shapes and nodal patterns, for a CSSF trapezoidal uniform plate with different thickness ratios $h_l = 0.001$, 0.2, are showed in Figs. 4 and 5. It can be observed that the thickness ratios have not a significant effect on the first four mode shapes.

Results that show the influence of the rotational and translational restrain parameters on the vibration behaviour of triangular plates are presented in two ways. In tabular form, this can be useful for benchmark comparison purposes and in graph form for a better understanding of the effect of the elastic restraints. The first five values of the frequency parameter $\Omega = \omega l^2\sqrt{\rho h^{(1)}/D^{(1)}}$ of an isosceles triangular plate with three edges elastically restrained against rotation $(R = R_2 = R_3 = R_4)$ and translation $(T = T_2 = T_3 = T_4)$ for two different thickness rations $h_l = 0.1$ and $h_l = 0.05$ are depicted in Tables 5 and 6, respectively. Figs. 6 and 7 show the variation of the first four frequency parameter Ω/π^2 for triangular and trapezoidal plates with different boundary conditions for various values of the elastic restraints. It can be observed that the major increase of frequency occurs when the translational elastic restrain values are in the interval (10–1000). The plate fundamental frequency is much less sensitive to such change. In general it is observed that the frequency parameter beyond a certain large value (say 10^4) the rate at which the frequency parameters approach the upper limit is relatively slow. This is almost certainly due to the nature of the stiff elastic restraints which are approaching the classical supporting edge conditions of the plate.

5. Conclusions

A simple, computationally efficient and accurate approximate approach has been developed for the determination of frequencies and modal shapes of free vibration of trapezoidal and triangular tapered thick plates. The methodology is based on the Ritz method and on the Reissner–Mindlin plate theory, and uses triangular coordinates to express the geometry of plate in a unified form. The transverse deflection and the rotations are approximated by sets of simple polynomials generated automatically.

The algorithm developed is very genera, functions extremely well and allows us to take into account a great variety of triangular and trapezoidal plates with any combination of boundary

Edge supports		Boundary conditions Free edge: $W \neq 0, \quad \phi_n \neq 0, \quad \phi_s \neq 0$ Simply supported edge: $W \neq 0, \quad \phi_n \neq 0, \quad \phi_s \neq 0$[a] Clamped edge: $W \neq 0, \quad \phi_n \neq 0, \quad \phi_s \neq 0$					
$u = 0$ $v = v\_0$	$u = 1$ $v = 1$	$p(u)_1^{(W)}$	$q(v)_1^{(W)}$	$p(u)_1^{(\phi)_x}$	$q(v)_1^{(\phi)_x}$	$p(u)_1^{(\phi)_y}$	$q(v)_1^{(\phi)_y}$
S	F	u	$v - v\_0$	1	$v - v\_0$	u	1
C	F	u	$v - v\_0$	u	v − v_0	u	$v - v\_0$
S	S	$u(u-1)$	$(v - v\_0)(v-1)$	1	$(v - v\_0)(v-1)$	$u(u-1)$	1
S	C	$u(u-1)$	$(v - v\_0)(v-1)$	$u-1$	$(v - v\_0)(v-1)$	$u(u-1)$	$v-1$
C	C	$u(u-1)$	$(v - v\_0)(v-1)$	$u(u-1)$	$(v - v\_0)(v-1)$	$u(u-1)$	$(v - v\_0)(v-1)$
F	F	1	1	1	1	1	1
F	S	$u-1$	$v-1$	1	$v-1$	$u-1$	1
F	C	$u-1$	$v-1$	$u-1$	$v-1$	$u-1$	$v-1$
C	S	$u(u-1)$	$(v - v\_0)(v-1)$	u	$(v - v\_0)(v-1)$	$u(u-1)$	$v - v\_0$

[a] φ_s denote the rotation about the normal direction n.

conditions including edges elastically restrained against rotation and translation and non-uniform cross sections.

Sets of parametric studies have been performed and the results have shown that the variation of the frequency with the taper parameter is linear for the first four modes and increases as the mode of vibration increases and the thickness ratios have not a significant effect on the first four mode shapes. On the other hand, when the translational elastic restrain values are in the interval (10–1000) it has been observed the major increase of frequency.

The authors believe that the approach should be well suited for optimisation problems of thick tapered isotropic plates due to its relative simplicity, both analytically and computationally, of varying the parameters involved.

Finally, it is important to point out that the method presented can be easily modified to be applied to static deflection problems and buckling analysis. On the other hand, the method can be generalized for analyzing anisotropic thick plates.

Acknowledgments

The present study has been sponsored by the PICTO – UNSa No. 36690. Ms V. Quintana has been supported by a CONICET fellowship.

Appendix A

Starting polynomials in the u and v co-ordinates for different combinations of classical boundary conditions.

References

[1] Leissa AW. Vibration of plates (NASA SP-160). Washington (DC): Office of Technology Utilization, NASA; 1969.
[2] Leissa AW. The free vibration of rectangular plates. J Sound Vib 1973;31:257–93.
[3] Leissa AW. Recent research in plate vibrations: classical theory. Shock Vib Dig 1977;9(10):13–24.
[4] Leissa AW. Recent research in plate vibrations, 1973–1976: complicating effects. Shock Vib Dig 1978;10(12):21–35.
[5] Leissa AW. Plate vibration research, 1976–1980: classical theory. Shock Vib Dig 1981;13(9):11–22.
[6] Leissa AW. Plate vibration research, 1976–1980: complicating effects. Shock Vib Dig 1981;13(10):19–36.
[7] Leissa AW. Recent studies in plate vibrations, 1981–1985. Part I: classical theory. Shock Vib Dig 1987;19(2):11–8.
[8] Leissa AW. Recent studies in plate vibrations, 1981–1985. Part II: complicating effects. Shock Vib Dig 1987;19(3):10–24.
[9] Reissner E. The effect of transverse shear deformation on the bending of elastic plate. J Appl Mech ASME 1945;12:69–76.
[10] Mindlin RD. Influence of rotary inertia and shear in flexural motion of isotropic, elastic plates. J Appl Mech ASME 1951;18:31–8.
[11] Liew KM, Xiang Y, Kitipornchai S. Research on thick plate vibration: a literature survey. J Sound Vib 1995;180(1):163–76.
[12] Karunasena W, Kitipornchai S, Al-bermani FGA. Free vibration of cantilevered arbitrary triangular Mindlin plates. Int J Mech Sci 1996;38(4):431–42.
[13] Karunasena W, Kitipornchai S. Free vibration of shear-deformable general triangular plates. J Sound Vib 1997;199(4):595–613.
[14] Wu L, Liu J. Free vibration analysis of arbitrary shaped thick plates by differential cubature method. Int J Mech Sci 2005;47:63–81.
[15] Zhong H Z. Free vibration analysis of isosceles triangular Mindlin plate by the triangular differential quadrature method. J Sound Vib 2000;237(4):697–708.
[16] Gorman DJ. Accurate free vibration analysis of shear-deformable plates with torsional elastic edge support. J Sound Vib 1997;203(2):209–18.
[17] Zhou D. Vibrations of Mindlin rectangular plates with elastically restrained edges using static Timoshenko beam functions with the Rayleigh–Ritz method. Int J Solid Struct 2001;38:5565–80.
[18] Malekzadeh P, Shahpari SA. Free vibration analysis of variable thickness thin and moderately thick plates with elastically restrained edges by DQM. Thin Wall Struct 2005;43:1037–50.
[19] Xiang Y, Liew KM, Kitipornchai S. Vibration analysis of rectangular Mindlin plates resting on elastic edge supports. J. Sound Vib 1997;204(1):1–16.
[20] Nallim LG, Luccioni BM, Grossi RO. A Rayleigh–Ritz approach to transverse vibration of isotropic polygonal plates with variable thickness. J Multi-body Dynam 2002;216:213–22.
[21] Gutierrez RH, Laura PAA. Fundamental frequency of transverse vibration of a rectangular, anisotropic plate of discontinuously varying thickness. J Sound Vib 2001;248:573–7.
[22] Mikhlin S. Variational methods of mathematical physics. New York: Mac Millan Co.; 1964.
[23] Maple User Manual. Toronto: Maplesoft, a Division of Waterloo Maple Inc.; 2005–2009.
[24] CSI Analysis Reference Manual. Berkeley, California, USA: Computers and Structures, Inc.; 2004.